Neutron study of mesoscopic magnetic clusters: $Mn_{12}O_{12}$

M. Hennion
Laboratoire Leon Brillouin (CEA-CNRS), CEA-Saclay, 91191 Gif-sur-Yvette, France

L. Pardi
National High Magnetic field Laboratory, Florida State University, 1800 E. Paul Dirac DR, Tallahassee, Florida 32306

I. Mirebeau
Laboratoire Leon Brillouin (CEA-CNRS), CEA-Saclay, 91191 Gif-sur-Yvette, France

E. Suard
Institut Laue-Langevin, Boîte Postale 156X, 38042 Grenoble Cedex, France

R. Sessoli and A. Caneschi
Department of Chemistry, University of Florence, Via Maragliano 77, 50144 Firenze, Italy
(Received 3 March 1997)

Neutron diffraction and inelastic neutron scattering in zero field have been performed on mesoscopic magnetic $Mn_{12}O_{12}$ clusters, well known for their macroscopic quantum effects observed at low temperature. In addition to the static spin correlations of the cluster in its ground state, we have observed some energy levels related both to the anisotropy and to the exchange energies of the cluster, with their respective dynamical form factor. The temperature and Q dependences of the anisotropy energy levels can be qualitatively explained using a quantum model. Besides these expected modes, the most striking result is the observation of extended energy modes at energy values below those related to anisotropy. Their temperature and Q dependences differ from those expected for the energy levels of usual magnetic clusters. They indicate an additional spin coupling which must play a role in tunneling properties. [S0163-1829(97)09534-9]

INTRODUCTION

Recently, superparamagnetic properties have been discovered at low temperature ($T<10$ K) for the magnetic clusters of formula $Mn_{12}O_{12}(CH_3COO)_{16}(H_2O)_4$.[1] These properties are associated with the existence of an energy barrier due to anisotropy with a strong uniaxial character. In contrast with the vast majority of superparamagnetic particles studied, these magnetic clusters are perfectly identical to each other so that they represent an ideal case for the study of relaxation or tunneling properties. They form a tetragonal lattice, the anisotropy being along the c axis. From low temperature susceptibility measurements, a total spin value $S=10$ was formulated for the ground state of the cluster, which can be depicted as a ferrimagnetic state with 8 Mn^{3+} ($S_a=2$) oriented antiparallel to 4 Mn^{4+} ($S_b=3/2$) as a result of the dominant exchange interactions.[2,3] A microscopic model of relaxation where the energy barrier is overcome via a coupling with phonons, has been proposed.[4,5] It uses a quantum picture, where the energy barrier consists in a staircase of energy levels corresponding to the splitting of the ground state $S=10$, by the magnetic anisotropy represented by a bilinear term DS_z^2. On the experimental side, very spectacular properties were recently found for the magnetization at low temperature, showing regular steps in the hysteresis cycle. They support the idea of a nearly perfect system for the study of macroscopic quantum tunneling[6–10] which, as a specificity of this system, appears thermally assisted. Since the uniaxial anisotropy does not allow transitions between the two $S=+10$ and $S=-10$ states, one has to understand the mechanism which allows the tunneling in such system. In this context, a microscopic study using neutron scattering can provide important informations. A first diffraction study was performed in applied field, indicating a large delocalisation of the electronic spin density.[11] In the present paper we report the first microscopic study in zero field of this system, in the energy range corresponding to anisotropy and first exchange levels. Actually, the neutron probe provides a direct observation of the imaginary part of the susceptibility $\chi''(Q,\omega)$ in an energy range corresponding to fluctuation times of about 10^{-10} to 10^{-12} s, far apart from the measurement times corresponding to relaxation or tunneling effects. Two different techniques were used. (1) By diffraction (without energy analysis), we have measured the spin correlations which at low temperature correspond to the time averaged magnetic spin structure of the $Mn_{12}O_{12}$ cluster. (2) By inelastic scattering we have measured the excitation spectra, in an energy range up to 7 THz. In these experiments, like in previous ones where generally much smaller clusters are investigated,[12] the quantum nature of the magnetic state of the cluster clearly appears in well defined energy levels. However, this microscopic study reveals the existence of extended energy states, with peculiar temperature and Q dependences. The paper is divided as follows: In Sec. I the observations obtained by diffraction and inelastic scattering are successively reported. In Sec. II, a qualitative analysis of the observations is proposed with a discussion concerning the new extended energy states. In Sec. III, we report a quanti-

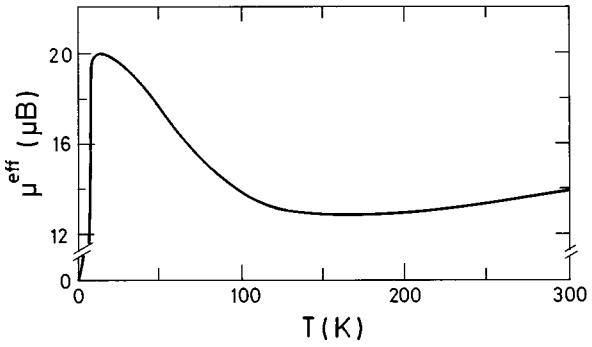

FIG. 1. Effective magnetization per cluster as a function of temperature.

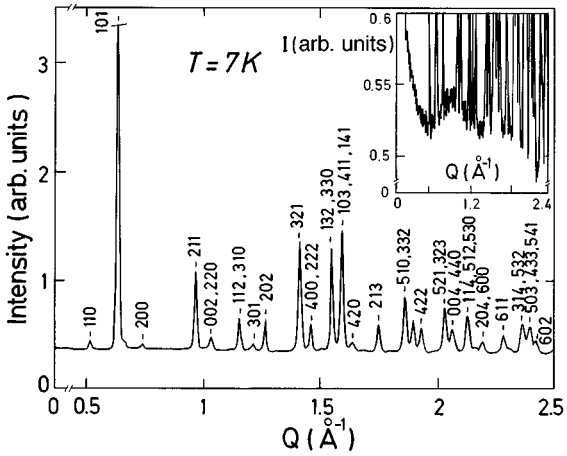

FIG. 2. Diffraction spectrum showing the nuclear Bragg peak intensities. In the inset, the intensity is increased by a factor of 10, showing the modulations of the diffuse intensity below the Bragg peaks.

tative analysis of the energy levels related to the anisotropy, using at first a quantum description within a simplified picture for the ground state of the cluster and then a classical approximation.

I. EXPERIMENT

A powder sample of $Mn_{12}O_{12}[C(D_{1-x}H_x)_3COO]_{16}[(D_{1-x}H_x)_2O]_4$ of about 1 g was prepared for the neutron experiments. The x parameter indicates that the deuteriation, intended to decrease the incoherent contribution of H, was only partly successful. The value of x was determined from the transmission factor of the direct neutron beam (see below).

The nuclear structure was first determined by x rays with a four circle spectrometer on a small single crystal. The data fully agree with the previous study of Lis[13] who has found a centered tetragonal structure with space group $I4$, and $a=17.319$ Å, $c=12.388$ Å as lattice parameters. ac susceptibility curves $\chi'(\omega)$, and $\chi''(\omega)$ were determined in a very low field (1 mT). From $T\chi'(\omega)$, the temperature dependence of the effective magnetization $\mu^{\text{eff}}(T)$ was deduced and reported in Fig. 1. The drop below 15 K indicates the onset of relaxation effects. The extrapolation of the linear portion below 40 K yields $\mu^{\text{eff}}=21\mu_B$, in good agreement with the expected $S=10$ value. This curve agrees very well with earlier measurements.[1–3]

A. Neutron diffraction study

The neutron diffraction measurements were carried out on the G6-1 spectrometer of the reactor Orphée (Laboratoire Léon Brillouin) with a multidetector, using the incident wavelength $\lambda=4.74$ Å. With two different positions of the detector, we could investigate the scattering vector Q range $0.2<Q<2.5$ Å^{-1}. The powdered sample, in a cylindrical holder of aluminium, was set in a cryogenerator. The spectra were recorded at five temperatures in the range $7\text{ K}<T<300$ K. The intensities were corrected from the detector cell efficiency and from the scattering of the sample holder, using the experimental determination of the transmission factor of the direct beam. From the comparison between the calculated and experimental transmission factor, taking into account the weight and density of the irradiated sample, we deduce the concentration of hydrogen, x, still present in the sample ($x\simeq 0.3$). The intensities were converted in barn/at/ster using a Vanadium of cylindrical shape, taking into account the angular dependent absorption and multiple scattering effects.

In Fig. 2, we have reported a typical scattering intensity observed at $T=7$ K. The position of the Bragg peaks can be indexed within the tetragonal structure. The indetermination about the relative D/H occupancies on the sites prevent to analyze their intensities. Interestingly, the Bragg peaks are superimposed on a large signal, which consists of a diffuse, smoothly Q-modulated component and of a Q-independent one, readily related to nuclear incoherent scattering (evaluated to 1.08 barn/average atom or 12 barn/Mn). This appears when looking at a much larger scale (see the inset of Fig. 2 for $T=7$ K where the scale has been increased by a factor of ten). This Q modulation evolves continuously with temperature between 7 and 300 K, indicating its magnetic origin. This magnetic intensity was approximated by a set of Tchebytcheff polynomials using a smoothing procedure from which one obtains the continuous curves reported on Fig. 3 at the two extremal temperatures, 7 and 300 K. At 7 K, this diffusive intensity shows a strong increase below $Q=0.4$ Å^{-1} and two rounded maxima at about $Q=0.8$ Å^{-1} and 1.8 Å^{-1}. At 300 K, the enhancement observed at small Q values has nearly disappeared. The small residual enhancement is attributed to powder grain scattering and therefore has been subtracted from the spectra at all temperatures, yielding the dashed curves in Fig. 3. The maximum at 0.8 Å^{-1} has also disappeared whereas a large bump still persists at 1.6 Å^{-1}.

B. Inelastic neutron scattering

Inelastic scattering experiments were carried out on the three axis spectrometers $4F1$ and $1T$, installed respectively on the cold and the thermal sources. Bent graphites were used as monochromator and analyzer. The energy scans were performed at constant outcoming neutron wave vector, mainly using $k_F=1.55$ Å^{-1} with a berylium filter, investigating the 0–3.5 THz energy range at various temperatures.

At low temperature, a typical energy spectrum can be divided into three parts: (i) a well defined excitation around

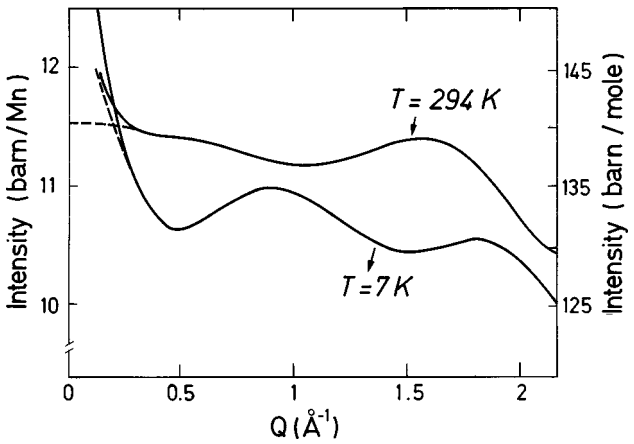

FIG. 3. The continuous curves represent the diffuse intensity at $T=294$ K and 7 K, obtained by a smoothing procedure from the raw data. The dashed part of the curves below $Q=0.25$ Å^{-1}, are obtained after the subtraction of the residual increase observed in this low-Q range at 294 K and attributed to the scattering by powder grains.

0.3 THz or 1.24 meV, (ii) a broad excitation spectrum around 0.2 THz, and (iii) another broad energy spectrum mainly between 1.2 THz up to about 7 THz. We describe their respective characteristics successively.

In Fig. 4 we have reported a typical inelastic scattering spectrum observed in the 0–0.5 THz range with neutron energy loss at $Q=0.95$ Å^{-1}, $T=1.55$ and 2.59 K. The huge central peak at $\omega=0$ is attributed mainly to the *elastic* incoherent nuclear contribution. We also observe a broad energy ''mode'' around 0.2 THz, whose intensity mainly increases between 1.55 and 2.59 K and a well defined peak at 0.3 THz. This latter inelastic peak can be fitted by a delta function convoluted with the spectrometer resolution, indicating a

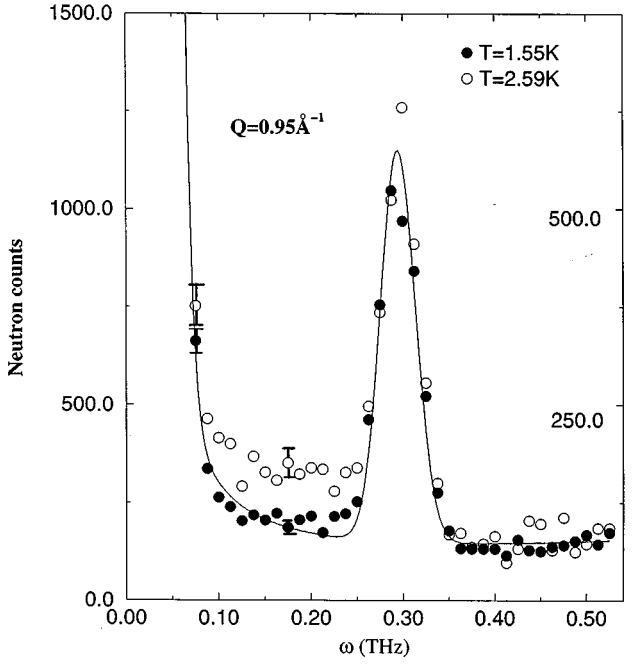

FIG. 4. Energy scan measured at $Q=0.95$ Å^{-1} and $T=1.55$ K, and 2.59 K. The continuous line is a fit using a delta function for the peak convoluted with the spectrometer resolution.

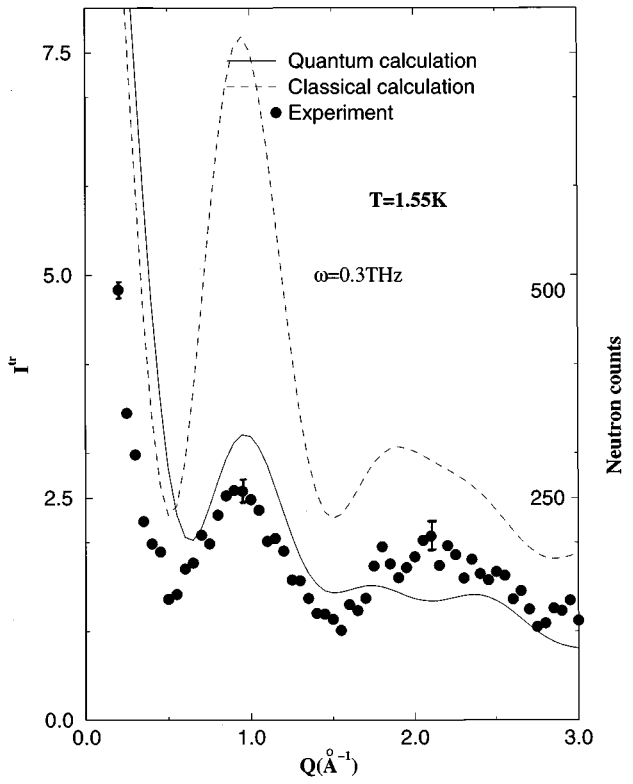

FIG. 5. Intensity obtained at constant energy ($\omega=0.3$ THz) versus Q. Full circles: experiment, in neutron counts (scale on the right side) and in μ_B^2/g^2 units (scale on the left side). The continuous and dashed lines correspond to the quantum and classical calculations, respectively. They both tend to the $13.333\mu_B^2/g^2$ value for $Q=0$.

well defined excitation energy at $\omega=0.3$ THz (1.24 meV). In Fig. 5 we have reported the Q dependence $I(Q)$ of the maximum peak intensity ($\omega=0.3$ THz), corrected from the background of the sample. This latter was obtained from the averaged intensities measured at $\omega=0.2$ and $\omega=0.4$ THz, namely just outside the peak. Such procedure is justified in the present case owing to the very low coherent intensity measured at these energies and temperatures (see below). In addition all the data at small Q values ($Q<0.05$ Å^{-1}) were checked by complete energy scan as that performed at $Q=0.95$ Å^{-1} (Fig. 4). As indicated by the scale on the left side, the data in Fig. 5 have been put on an absolute scale (corresponding to μ_{B^2}/g^2 units) using the incoherent scattering of a vanadium sample. There can be a systematic error, estimated as 30% of the intensity, mainly due to the determination of the sample transmission. The intensity $I(Q,\omega=0.3\,\text{THz})$ shows large modulations with minima and maxima at the same Q values as those of the magnetic intensity observed in the diffraction experiment (inset of Fig. 2). The first maximum is observed for $Q=0.95$ Å^{-1}.

In Fig. 6, the energy line shape measured around $\omega=0.3$ THz and at $Q=0.95$ Å^{-1} is reported at four temperatures between 1.5 and 17 K. As the temperature rises, the intensity of the inelastic peak decreases and broadens on its low-energy side. Moreover, we still observe some bump around 0.2 THz.

To understand better the origin of this broad energy ''mode'', we have performed a detailed study of its temperature and Q dependences. Q scans performed at $\omega=0.2$ THz,

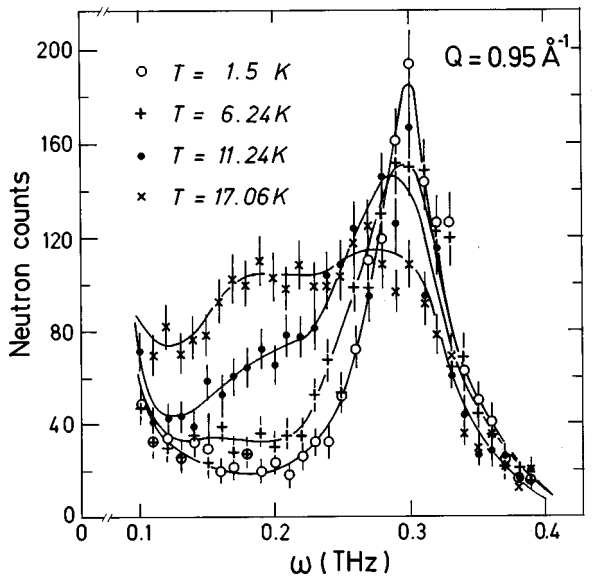

FIG. 6. Energy scans at constant Q (0.95 Å^{-1}) and at four temperatures: 1.5, 6.24, 11.24, and 17.06 K. The continuous lines are guides for the eyes.

for several temperatures, are reported in Fig. 7. With respect to the energy mode at 0.3 THz, we observe important differences: (i) The intensity of this ''mode'', which already exists at the very low temperature value 1.55 K, as indicated by the Q dependence of the intensity, fastly increases in a low and narrow temperature range. Note the difference between 1.55 and 2.1 K, compared to that between 2.1 and 2.77 K. The variation of the intensity of this ''mode'' cannot be followed above this temperature, since the increase of the intensity (reported in Fig. 6 for instance) becomes dominated by the contribution of the anisotropy levels as shown below. (ii) The low Q intensity is temperature independent, which suggests that it is of purely nuclear origin, in contrast with the mode at 0.3 THz which shows a huge magnetic intensity at low Q. Therefore, the Q modulation related to this ''mode'', is very different from that observed at 0.3 THz, showing mainly a broad Q modulation with a first maximum at $Q=1.18$ Å^{-1} instead of 0.95 Å^{-1} (compare Figs. 5 and 7 reported with the same Q scale), and no intensity around $Q=0$.

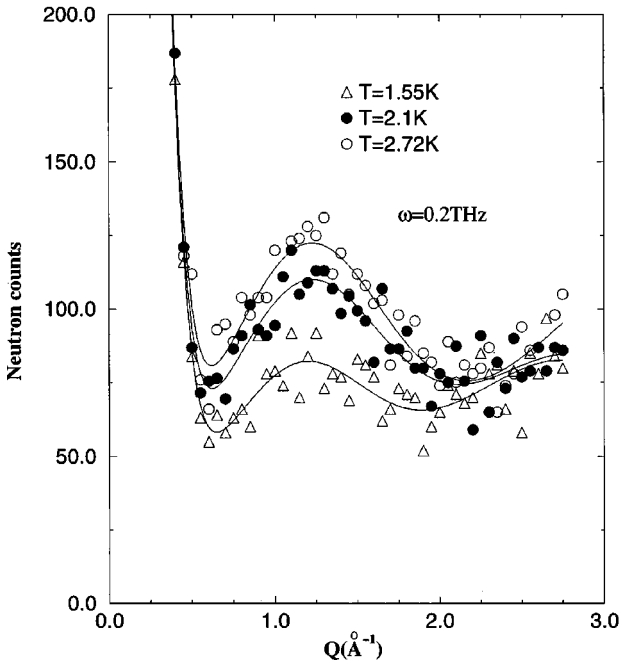

FIG. 7. Q dependence of the intensity obtained at $\omega=0.2$ THz at three temperatures. The continuous line is a guide for the eye.

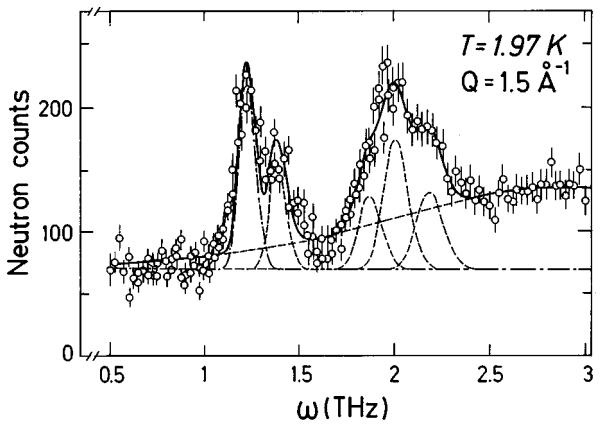

FIG. 8. Energy scans at constant Q (1.5 Å^{-1}) and $T=1.97$ K. The dashed lines correspond to a fit with calculated functions (see the text).

At higher energies, in the 0.5–3 THz energy range, we observe new excitations. They are shown in Fig. 8 for a Q value of 1.5 Å^{-1}. Several peaks are superimposed over a broad mode. The data can be fitted using delta functions for the narrow peaks (five at least), a Lorentzian line shape for the broad mode (centered at 3 THz) and a constant energy background, all of them being convoluted with the spectrometer resolution. The narrow peaks are perfectly fitted indicating well defined excitations. The Q dependence of the energy level $\omega=1.2$ THz, corresponding to one of the well-defined peaks of Fig. 8, is reported in Fig. 9 exhibiting several modulations. Above 3 THz, the intensity of the broad mode smoothly decreases, as observed when using a higher wave vector for outcoming neutrons ($k_F=2.662$ Å^{-1}). However, at very high energies, the poorer energy resolution prevents a clear observation of eventual additional peaks.

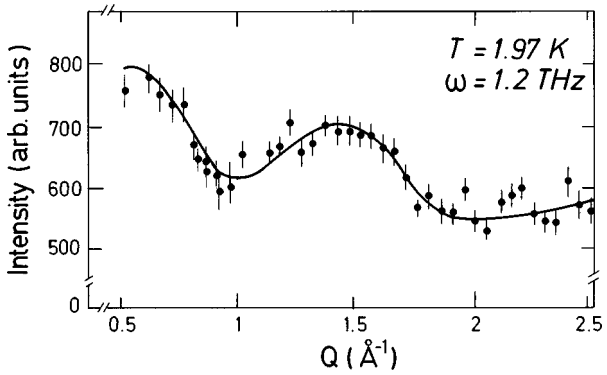

FIG. 9. Intensity at constant energy ($\omega=1.2$ THz) versus Q. These data have been obtained using $k_F=2.662$ Å^{-1}. The intensities have been normalized in the Q range 0.5–1 Å^{-1}.

II. QUALITATIVE ANALYSIS

First, we qualitatively discuss our observations, considering (1) the diffuse intensity measured by diffraction, (2) the excitation around 0.3 THz, (3) the broad spectrum around 0.2 THz, and finally (4) the spectrum at higher energy successively.

(1) The diffuse magnetic scattering measured by diffraction shown in Fig. 3 corresponds to an integration over the energies. On the side of neutron energy gain, this integration extends over all thermally populated energy levels whereas for neutron energy loss, the integration is truncated at the incident energy ($\lambda = 4.74$ Å corresponds to $E_i = 0.87$ THz). At 7 K, where the transitions within both anisotropy and exchange levels are not excited, this intensity is essentially ''elastic'' and corresponds to the Fourier transform of the correlations $\langle S_i^z S_j^z \rangle$, where z is the anisotropy axis, that we call ''longitudinal'' below. Assuming that there is no interaction or correlation between the clusters spins (the dipolar forces are negligible), the directions of the resultant cluster spins vary randomly between $+z$ or $-z$ between the various clusters within a single crystal grain. Therefore, the spin correlations $\langle S_i^z S_j^z \rangle$ can be calculated for spins of individual clusters and added independently. Such calculation is performed in Sec. III B, and confirms this interpretation. As the temperature increases, the anisotropy and the exchange excitations are progressively integrated in the measurement, so that the Q dependence evolves. At 300 K, the bump observed around 1.6 Å^{-1}, being absent at 7 K, is attributed to residual antiferromagnetic correlations inside one cluster, and therefore indicates the existence of an exchange coupling value of at least 25 meV in this system. This latter conclusion is consistent with the magnetization measurements (Fig. 1), where the values at 300 K ($14\mu_B$) are much lower than the value for the true paramagnetic state ($19.5\mu_B$) given by the sum of independent spin contributions inside each cluster: $(\mu^{\text{eff}})^2 = 4g^2 S_a(S_a+1) + 8g^2 S_b(S_b+1)$ ($g=2$, $S_a = 3/2$, and $S_b = 2$).

This situation differs from that where a long range ferromagnetic order is induced between the clusters by applying a magnetic field.[9] There, the Fourier transform of the magnetic distribution is only visible at the Bragg peak positions.

(2) The excitations around 0.3 THz are the most important ones to understand the relaxation properties of these clusters. The well defined excitation observed at $\omega = 0.3$ THz (1.24 meV) as shown in Fig. 4 is in perfect agreement with the value of anisotropy previously determined by EPR using very high magnetic fields.[2] In the assumed model of dominant exchange interactions, the ground state of the cluster $S = 10$, $M = \pm 10$, is splitted in zero field due to the single ion anisotropy in a series of 11 levels corresponding to the S^z component ranging from $M = \pm 10$ to $M = 0$. At 1.55 K only the ground state is populated. Then, only one possible transition, satisfying the selection rule given by the neutron cross section ($\Delta M = +1, -1$), can be observed, with the maximum intensity. With the assumption of a single quadratic term DS^{z2}, the peak provides a value $D = 0.52$ cm^{-1} or 0.77 K for the anisotropy constant, which is significantly larger than the 0.46 cm^{-1} value determined from the macroscopic magnetization measurements.[7–9] When the temperature increases, new transitions are allowed with smaller energy values such as $\omega = D[(S^z-1)^2 - (S^z-2)^2]$, etc. Since the resolution energy, given by the observed linewidth of the peak, does not allow to separate two levels (distant from $2D = 0.03$ THz or 0.13 meV), we expect a progressive broadening of the energy line shape on its low energy side, with a decrease of the intensity at 0.3 THz due to the conservation of the total magnetic intensity. These features are qualitatively observed in Fig. 6. However, the decrease of the intensity at 0.3 THz with temperature (see Fig. 6) is faster than that predicted with a uniaxial DS^{z2} as calculated in Sec. III A 1, indicating that the energy levels which appear by thermal population are smaller than expected. Moreover, some intensity is observed below 0.3 THz (see Fig. 6) which cannot originate from the 0.3 THz level as discussed in (3). On the other hand, the Q dependence of the $\omega = 0.3$ THz intensity, at a given temperature (Fig. 4), can be qualitatively interpreted along the above splitting scheme as calculated below Sec. III A 2, which confirms the nature of this excitation.

(3) The broad energy ''mode'' around 0.2 THz (Fig. 7) is the most surprising result since it was not expected by previous measurements. In particular it cannot be related to the anisotropy excitations. Its main features can be summarized as follows.

(i) The very large extension of this ''mode'' contrasts with the well defined magnetic excitations observed in the highest energy range (see Fig. 4). (ii) Its temperature dependence is not related to a Boltzmann population factor as observed for all other modes, and shows a change of regime around 2K. (iii) Its Q dependence is clearly distinct from other modes, with a first maximum at a higher Q value and no magnetic intensity around $Q = 0$. These observations lead to the following comments.

This ''mode'' has a magnetic origin (phonons would exhibit a Q^2 dependence) and since observed at rather large Q values, suggests that the involved spins are coupled on a local scale. The Q dependence (Fig. 7) is characteristic of an excitation of a dimer with an antiterromagnetic coupling. It leads to a $[1+(-1)^{S-S'}\cos(QR)]$ (Ref. 14) law, which for $S - S' = 1$, goes to zero at $Q = 0$. This law used in the fit of Fig. 7 determines a distance R of 2.66 Å, close to the distance 2.76 Å of the $Mn^{3+}-Mn^{4+}$ pairs of atoms bridged by oxygens. The very large energy linewidth could be related to a very short lifetime or to a distribution of energy levels. On the other hand, the peculiar temperature dependence of the intensity, with a marked increase up to 2 K, indicates that these excitations do not originate from the lowest ground state, but from some energy level located mainly around 0.03 THz (0.12 meV) or 2 K from the ground state. The study of this lower energy mode, not observable in the present experimental conditions is actually in progress. We emphasize that the increase with temperature of the intensity takes place in the temperature range where the tunneling properties are observed, so that we believe that these new excitations could play an important role in the physical process involved. In particular the fast increase around 2 K is reminiscent of the decrease of the first field value observed above 2 K in Ref. 8, Fig. 2. Since this ''mode'' lies at a lower energy than the first anisotropy level, it must contribute to decrease the energy barrier as it becomes thermally populated and therefore can be one of the origins leading to a discrepancy between

the microscopic and macroscopic determination of the anisotropy (0.61 and 0.77 K from the present study).

(4) In the higher energy range, the two main peaks around 1.2 and 2.2 THz are attributed to magnetic excitations related to exchange coupling between the spins of one cluster. In the model previously proposed to interpret the temperature dependent susceptibility[15] two degenerated $S=9$ states were calculated at 0.725 THz, one $S=8$ at 1.195 THz and other $S\leqslant 8$ or $S>10$ states at higher energies. The mode at 0.725 THz is hardly visible here (possibly due to a very small intensity at this Q value) whereas the one at 1.2 THz is well observed. However, due to the neutron selection rules, $\Delta S=0,\pm 1$, $\Delta M=0,\pm 1$, one could only expect transitions from the ground state $S=10$, $M=10$ to the $S=9$, $M=9$ and to the $S=11$, $M=10$, and $M=11$ states, so that the transition to $S=8$ is in principle forbidden. Another surprising result is the observation of a splitting of the two main modes into several well defined modes, possibly two or three around 1.2 THz and 3 around 2 THz. All these features indicate that the ground state is not a single $S=10$, $M=10$ state, but a more complex one, due to some additional coupling not included in the simple model of exchange and uniaxial anisotropy.

III. EXCITATIONS RELATED TO THE ANISOTROPY: A QUANTITATIVE COMPARISON

In this last part, we focus on the observations related to the anisotropy energy only and we show to what extent we are able to interpret the observed temperature and Q dependences. We use the simple model of cluster with exchange and bilinear term of anisotropy, neglecting all the peculiar dynamical features detailed in Sec. II.

From the general expression of the neutron scattering cross section,[16] we can write

$$\begin{aligned}\frac{d^2\sigma}{d\Omega d\omega}(\mathbf{Q},\omega) = A[1/2gF(Q)]^2 1/Z \\ \times \exp([(E(S,M')-E(S,M)]/k\mathbf{T}) \\ \times \sum_{\alpha,\beta}(\delta_{\alpha,\beta}-Q^\alpha Q^\beta/Q^2) \\ \times \sum_{i,j}\exp[i\mathbf{Q}(\mathbf{R}_i-\mathbf{R}_j)] \\ \times \sum_{M,M'}\langle SM|S_i^\alpha|SM'\rangle\langle SM'|S_j^\beta|SM\rangle \\ \times \delta[\omega-E(S,M)-E(S,M')]. \qquad (1)\end{aligned}$$

Here, A is a constant $[=N(\gamma e^2/2mec^2)]$, with N the number of $Mn_{12}O_{12}$ molecules] α,β $(=x,y$ or $z)$ refer to the cartesian coordinates (z being along the uniaxial anisotropy c axis), i,j run over the 12 spins of the cluster, located at positions $\mathbf{R}_i$, $F(Q)$ is the form factor of Mn ions (in the following, the form factor of Mn^{3+} only was used), $E(S,M)$ is the energy of the magnetic cluster state $|S,M\rangle$ and Z is the partition function. In this expression, only transitions between values of M are considered, S keeping the value $S=10$. This assumption is clearly valid up to about 20 K, as indicated by the energy values of the excitations attributed to exchange.

A. Excitations related to the anisotropy or "transverse spin fluctuations"

In the present assumption of a splitting by an uniaxial anisotropy along z, we consider only the spin components with $\alpha=\beta=x$ and $\alpha=\beta=y$ in Eq. (1).

1. Temperature dependence of the intensity

We first consider the temperature dependence of the anisotropy excitations for which the calculation of the matrix elements is straightforward. From Eq. (1), the Q dependence of the intensity, $I^{\mathrm{tr}}(Q,\omega)$, depends on the temperature through a scale factor only. Therefore we can obtain the relative temperature dependence of the intensity, considering an arbitrary Q value. In particular $I^{\mathrm{tr}}_Q(\omega,T)\propto I^{\mathrm{tr}}_{Q=0}(\omega,T)$. At $Q=0$ the summation over i and j in Eq. (1) is readily performed. We have for the x component (and identically for y)

$$\begin{aligned}\sum_{i,j}\sum_{M,M'}\langle SM|S_i^x|SM'\rangle\langle SM'|S_j^x|SM\rangle \\ = \sum_{MM'}\langle SM|\sum_i S_i^x|SM'\rangle\langle SM'|\sum_j S_j^x|SM\rangle \\ = \sum_{M,M'}\langle SM|S^x|SM'\rangle\langle SM'|S^x|SM\rangle, \qquad (2)\end{aligned}$$

where $S^x=\Sigma_i S_i^x=\Sigma_j S_j^x$ is now the x component of the *total* spin of the cluster. The calculation of the matrix elements is then straightforward, using $S^x=0.5(S^+ + S^{-1})$, $S^y=(0.5/i)(S^+-S^-)$ and $S^+|S,M\rangle=(S(S+1)-M(M+1))^{1/2}|S,M+1\rangle$, $S^-|SM\rangle=(S(S+1)-M(M-1))^{1/2}|S,M-1\rangle$. Since $M'=M-1$, we obtain

$$\begin{aligned}\langle SM|S^x|SM'\rangle\langle SM'|S^x|SM\rangle+\langle SM|S^y|SM'\rangle\langle SM'|S^y|SM\rangle \\ = S(S+1)-M(M+1). \qquad (3)\end{aligned}$$

We have calculated the line shapes $I^{\mathrm{tr}}(\omega)$ at a constant Q using Eqs. (1) and (3). The intensities shown in Fig. 10 as a function of temperature are obtained by using a Gaussian function [instead of the delta function of Eq. (1)] to take into account the spectrometer resolution. The normalization of the Gaussian (amplitude and linewidth) is made at 1.54 K. When the temperature increases, the general experimental tendency is of course observed. However, as mentioned in the qualitative interpretation, one observes that the main experimental peak broadens and its intensity decreases *much faster* with temperature than the calculated curve, indicating that the energy levels are smaller than predicted. This agrees with recent EPR experiments[17] which are interpreted by introducing higher order terms in the anisotropy. This discrepancy can partly explain the difference between the energy barrier value extracted from the Arrhenius law[1] or determined from the resonant tunneling effects[7–10] ($\Delta=DS^2=61$ K, $S=10$) and that deduced from the lowest level at 0.3 THz when using a quadratic anisotropy energy only (77 K). Besides this effect, we recall that the unexpected level around 0.2 THz could play some role in the variation of the intensity, considering that the total magnetic intensity must be conserved with temperature.

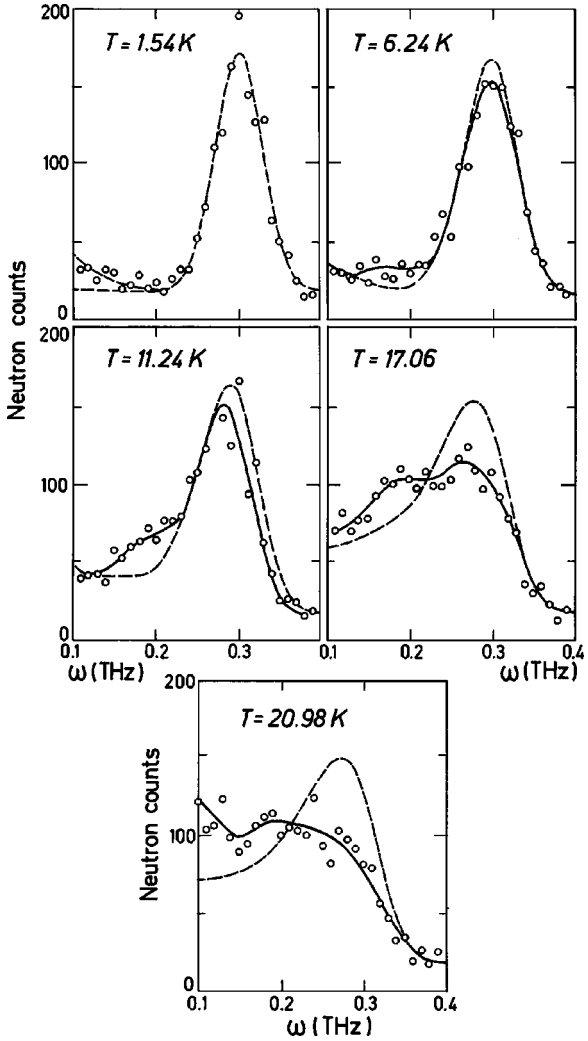

FIG. 10. Comparison between the observed and calculated profiles of the energy scans corresponding to the anisotropy excitations at four temperatures. The continuous lines through the experimental points are guides for the eyes (identical to those of Fig. 6). The dashed lines corresponds to the calculation (see the text). At all temperatures $T>2$ K, the tail of the central peak observed below 0.2 THz (determined at 2 K from the difference between the two dashed lines), has been added to the calculated functions.

2. Q dependence of the intensity

By contrast with the temperature dependence of the energy spectrum, the Q dependence of the intensity for a given excitation asks for the knowledge of the $S=10$ ground state (eigenvalues *and* eigenvectors). One has to calculate the $\langle \sigma SM|S_i^{\alpha}|\sigma SM'\rangle$ matrix elements for each $|\sigma SM\rangle$ to $|\sigma SM'\rangle$ transitions between the anisotropy levels. Here S and M are the total spin quantum number and its component along the quantization axis, respectively. σ stays for all the intermediate spin quantum numbers necessary to univocally define the spin function according to the coupling scheme of Fig 11. Any other coupling scheme would be equivalent (related by a unitary transformation). In fact, this particular one is the most appropriate under the assumption of a dominant antiferromagnetic J_1 exchange constant for the $Mn^{3+}-Mn^{4+}$ pairs (corresponding to bis-μ-oxo bridges). As already mentioned, one assumes[15] that the ground state and the excited states at low enough energy correspond to spin states which fulfill the condition

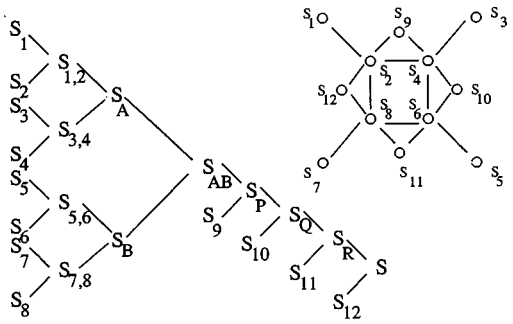

FIG. 11. Scheme of coupling (I) of the spins of the cluster Mn_{12} used for the calculation of the matrix elements. The local spins of the cluster have been labeled according to the simplified drawing of the cluster shown above the scheme. There, the spins labeled S_2, S_4, S_6, and S_{10} correspond to $Mn^{4+}(S_b=3/2)$ and the remaining spins to $Mn^{3+}(S_a=2)$.

$$S_{1,2}=S_{3,4}=S_{5,6}=S_{7,8}=1/2. \tag{4}$$

This assumption corresponds to consider J_1 as infinite and to completely disregard all the spin configurations which violate Eq. (4). It greatly reduces the number of states and makes the calculation of thermodynamical and spectroscopic properties manageable. A unique set of exchange constants was found which provide the $S=10$ state as a ground state of the cluster and allowed to fit the susceptibility in the low temperature range.[2] Any coupling scheme other than the one depicted in Fig. 11 will not satisfy the condition (4) as explained in Ref. 18.

Thus using this spin function for the $S=10$ ground state, the matrix elements $\langle \sigma SM|S_i^{\alpha}|\sigma SM'\rangle$ were readily calculated through the Wigner-Eckart theorem using the irreducible tensor operator technique[19] for the calculation of reduced matrix elements. $I^{\mathrm{tr}}(Q)$ is then obtained from Eq. (1), after performing an average over all the Q directions with respect to the crystallographic axis c.

In Fig. 5, $I^{\mathrm{tr}}(Q)$ is compared with the experimental data, put in the same μ_B^2/g^2 units. We note that the intensity at $Q=0$ is determined by S and M values only: $I^{\mathrm{tr}}(Q=0)=2/3\ [S(S+1)-M(M+1)]=13.33$ (with $S=10$, $M=9$, and the factor 2/3 related to the average over the **Q** orientations) and therefore independent on the model. The positions of the minima and maxima are well reproduced, confirming the origin of the excitation. The discrepancy with experiment is mainly observed at low Q, and at the second Q modulation showing the limits of this simple model.

B. ''Static'' or longitudinal spin correlations

The same comparison could be performed in principle with the ''static'' spin correlations in the ground state as observed by diffraction at low temperature. We have to consider $\alpha=\beta=z$ and $E(S,M)=E(S,M')$ in Eq. (1), and then to calculate the matrix elements

$$\Sigma_{i,j}\Sigma_{M,M'}\langle SM|S_i^z|SM'\rangle\langle SM'|S_j^z|SM\rangle.$$

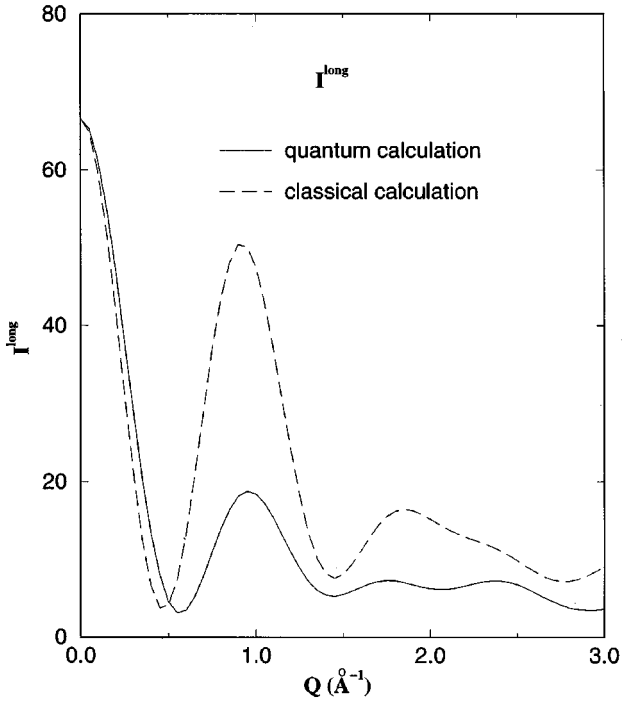

FIG. 12. Comparison between the quantum calculation and the classical model for longitudinal correlations $I^{\text{long}}(Q)$ in μ_B^2/g^2 units.

Using the same approximation as for the transverse excitations (J_1 infinite), and performing a powder average, one obtains the ''longitudinal'' intensity $I^{\text{long}}(Q)$ shown in Fig. 12. At $Q=0$, $I^{\text{long}}(Q)=2/3(S^z)^2=66.6$. We have not compared quantitatively the calculation to the experimental curve shown in Fig. 3 due to the difficulty to extract the magnetic component from the total experimental intensity. (The huge nuclear contribution is evaluated to 90% of the total intensity at $Q=0$).

C. Classical approximation

Although a classical calculation of the structure is incorrect since it ignores the quantum nature of the cluster ground state, we can expect that it provides an interesting approximation in the present case due to the rather large number of spins involved. For instance, considering the local spins in Eq. (1) as vectors rather than operators, we replace $\Sigma_{i,j}\Sigma_{M,M'}\langle SM|S_j^x|SM'\rangle\langle SM'|S_j^x|SM\rangle$ by $\Sigma_{i,j}S_i^xS_j^x$ in Eq. (1) (resp. for y component). The spin components are defined by a perfect ferrimagnetic arrangment which provides a total $S=10$ value. Performing an average over all the **Q** directions we obtain

$$I^{\text{tr}}(Q)=1/(4\pi)F(Q)^2\int_0^{2\pi}d\theta\int_0^{\pi}d\varphi\ \sin\varphi[1-0.5\sin^2(\varphi)]. \tag{5}$$
$$\left(\left[\sum_{i=1,12}S_i^{\text{tr}}\cos(\mathbf{QR}_i)\right]^2+\left[\sum_{i=1,12}S_i^{\text{tr}}\sin(\mathbf{QR}_i)\right]^2\right).$$

Here, θ and φ are the Euler angles which define the **Q** direction with respect to the cell axis in a single cristal. In this classical approximation, S_i^{tr} is the projection of the spin S_i in the plane perpendicular to the z anisotropy axis, with S^x and S^y component. At $Q=0$, for the first excitation ($S^z=9$), Eq. (5) provides the same limit as the quantum calculation: $I^{\text{tr}}(Q=0)=2/3[(\Sigma_iS_i^x)^2+(\Sigma_iS_i^y)^2]=2/3(S^2-S^{z2})=13.33$, where S^z is the z component of the total cluster spin. The comparison with the experiment is shown in Fig. 5 (dashed line). Although the position of minima and maxima are well reproduced, the huge intensity obtained on the first modulation peak (7.5 instead of 2.6 for the experiment) strongly disagrees with the experiment. We can easily conclude that the quantum calculation provides an important improvement compared to the classical approximation, even for such a large cluster. The same ''classical'' approximation can be also performed for calculating the ''static'' spin correlations in the ground state. Putting $\alpha=\beta=z$, and replacing the spin operators S_i^z by vectors, we obtain after powder average

$$I^{\text{long}}(Q)=1/(4\pi)F(Q)^2\int_0^{2\pi}d\theta\int_0^{\pi}d\varphi\ \sin^3(\varphi)$$
$$\times\left(\left[\sum_{i=1,12}S_i^z\cos(\mathbf{QR}_i)\right]^2+\left[\sum_{i=1,12}S_i^z\sin(\mathbf{QR}_i)\right]^2\right).$$

The corresponding Q dependence is compared to the quantum model in Fig. 12. These Q dependences are very similar to those found for the ''transverse'' spin correlations.

CONCLUSION

We have reported the first microscopic study in zero field of the mesoscopic $Mn_{12}O_{12}$ clusters, which is presently the subject of an intensive research work due to its macroscopic quantum tunneling effects, by investigating the energy range corresponding to anisotropy and first exchange levels. We show that some excitations can be unambiguously attributed to the anisotropy energy, and other ones to the intracluster modes, related to the formation of a large quantum spin state by coupling the spins of one cluster together. However, many features indicate a much more complex and rich situation in the dynamics of this system. For instance, the intensity of the excitations related to the anisotropy decreases faster than expected as temperature increases when using a bilinear form of the anisotropy energy. This observation which agrees with very recent EPR experiments performed in high field,[17] can partly explains why the anisotropy barrier value (61 K) deduced from relaxation properties or tunneling effects is smaller than that deduced from the first observed excited state (77 K) assuming a DS^{z2} energy. A multiplicity of exchange levels are observed in violation with the usual neutron selection rules. However, the most intringuing feature is the observation of a broad energy spectrum around 0.2 THz, therefore well below the first excited anisotropy level. This observation leads to the conclusion that there is a coupling inside the Mn_{12} cluster in addition to the direct exchange leading to the observed high energy levels or to the

spin orbit coupling leading the anisotropy. Even though the origin of this mode is not elucidated here, the peculiar dependence of its intensity in the temperature range where the tunneling properties are observed could suggest that it is an important key to understand the microscopic mechanism leading to quantum tunneling effects.

ACKNOWLEDGMENTS

The authors are very indebted to L. Puech and J. L. Tholence who have carried out the magnetization measurements in a very low field. They are very grateful to J. Villain, B. Barbara, A. Furrer, H. Casalta, and D. Gatteschi for stimulating discussion.

[1] R. Sessoli, D. Gatteschi, A. Caneschi, and M. A. Novak, Nature (London) **365**, 141 (1993).

[2] A. Caneschi, D. Caneschi, A. Sessoli, A. L. Barra, L. C. Brumel, and M. Guillot, J. Am. Chem. Soc. **113**, 5873 (1991).

[3] R. Sessoli, H. L. Tsai, A. R. Schake, S. Wang, J. B. Vincent, K. Folting, D. Gatteschi, G. Christou, and D. N. Hendrickson, J. Am. Chem. Soc. **115**, 1804 (1993).

[4] J. Villain, F. Hartmann-Boutron, R. Sessoli, and A. Rettori, Europhys. Lett. **27**, 15 (1994).

[5] P. Politi, A. Rettori, F. Hartmann-Boutron, and J. Villain, Phys. Rev. Lett. **75**, 537 (1995).

[6] B. Barbara, W. Wernsdorfer, L. C. Sampaio, J. G. Park, C. Paulsen, M. A. Novak, R. Ferre, D. Mailly, R. Sessoli, A. Caneschi, K. Hasselbach, A. Benoit, and L. Thomas, J. Magn. Magn. Mater. **140-144**, 1825 (1995).

[7] J. Friedman, M. P. Sarachik, J. Tejada, J. Maciejewski, and R. Ziolo, Phys. Rev. Lett. **76**, 3820 (1996).

[8] L. Thomas, F. Lionti, R. Ballou, D. Gatteschi, R. Sessoli, and B. Barbara, Nature (London) **383**, 145 (1996).

[9] J. M. Hernandez *et al.*, Europhys. Lett. **35**, 301 (1996).

[10] E. M. Chudnovsky, Science **274**, 938 (1996).

[11] P. A. Reynolds, E. P. Gilbert, and B. N. Figgins, J. Am. Chem. Soc. Inorg. Chem. **35**, 545 (1996).

[12] See, for instance, M. A. Aebersold, H. Blank, B. Briat, A. Furrer, and H. Güdel, Inorg. Chem. **30** (1991).

[13] X. Lis, Acta Crystallogr. Sect. B **36**, 2042 (1980).

[14] H. U. Güdel, A. Furrer, and J. K. Kjems, J. Magn. Magn. Mater. **54-57**, 1453 (1996).

[15] A. Caneschi, D. Gatteschi, L. Pardi, and R. Sessoli, in *Perspectives on Coordination Chemistry*, edited by A. F. Williams, C. Floriani, and A. E. Merbach (VCH, Basel, 1992).

[16] H. U. Güdel, A. Stebler, and A. Furrer, Inorg. Chem. **18**, 1021 (1979).

[17] A. L. Barra, D. Gatteschi, and R. Sessoli, Phys. Rev. B **56**, 8192 (1997).

[18] For example, we could couple first the $S=2$ spins of the crown of the cluster to give a total spin $S_{\text{crown}}=16$ and then the four spin $S=3/2$ of the core to give a total $S_{\text{core}}=6$, that we call scheme II in the following. The ground state $S=10$ can be found under the condition $S=S_{\text{crown}}-S_{\text{core}}$, but the assumption of a dominant J_1 cannot be easily taken into account. In order to confirm this idea we used both schemes I (Fig. 11) and II (defined in the text) to exactly calculate the eigenvalues and eigenvectors of the isotropic Hamiltonian $H=\Sigma\, J_{i,j}S_iS_j$ for a simplified cluster. The $S_a=2$ and $S_b=3/2$ spin values of the original cluster were replaced by the $S_a=1$ and $S_b=1/2$ values, respectively. For a set of exchange constants we found the $S=6$ ground state with the same spectrum of energy. However, when using scheme I, the set of eigenvectors mainly consists of spin functions corresponding to condition (4), whereas within the scheme II, it consists of a linear combination of various spin configurations, with non-negligible coefficients.

[19] B. L. Silver, *Irreducible Tensor Method* (Academic Press, New York, 1976).